Article

Not peer-reviewed version

Study on Electrochemical Behavior of Pyrite Oxidation in Alkaline Electrolyte

Yehao Huang , Zipei Jia , Wen Wang , Jia Yao , Runbo Gao , Laifu Xu , Hongtao Zhang , Yongsheng Zhang , Xiangyu Song *

Posted Date: 6 July 2023

doi: 10.20944/preprints202307.0388.v1

Keywords: Pyrite; Alkaline oxidation; Electrochemical technique; Surface passivation

Article

Study on Electrochemical Behavior of Pyrite Oxidation in Alkaline Electrolyte

Yehao Huang [1,3], Zipei Jia [1],Wen Wang [1], Jia Yao [1], Runbo Gao [1], Laifu Xu [1], Hongtao Zhang [1], Yongsheng Zhang [1] and Xiangyu Song [1,2,*]

[1] School of chemical engineering, Zhengzhou University, Zhengzhou 410001, PR. China
[2] Zhongyuan Critical Metals Laboratory, PR. China
[3] Henan Academy of Geology, Zhengzhou 450016, PR.China
* Correspondence: sxy5268@163.com (X. Song)

Abstract: Nowadays, the world's refractory gold ore production accounts for about 30% of the world's total gold, such gold concentrate leaching rate is low, seriously limiting the efficient use of gold resources. The alkaline preoxidation process can improve the leaching rate of this kind of gold deposit, and has a good development and application prospect. So, it is of great significance to study the oxidation and dissolution behavior of pyrite in alka-line environment. In this paper, the oxidation process of gold-bearing pyrite in alkaline electrolyte was studied by electrochemical techniques, and the oxidation products of pyrite electrode in alkaline solution were characterized by XPS，SEM and other analytical methods. The results show that the optimum pH for pyrite electrochemical oxidation dissolution is about 12, and oxidation potential of pyrite should be above 0.8 V. In that proces of alkaline oxidation dissolution of pyrite, part of S element enters the electrolyte in the form of S_x^{2-}, $S_2O_3^{2-}$, $SO_3^{2-}$and SO_4^{2-}, and a small amount of S element is adsorbed on the surface of the electrode in the form of S0 and becomes a part of the passive layer. Fe element is adsorbed on the surface of electrode in the form of $Fe(OH)_2$, Fe_2O_3 and $Fe_2(SO_4)_3$, which becomes the main component of passivation layer. This study provides a theoretical basis and reference data for the chemical preoxidation treatment of sulfide ores.

Keywords: pyrite; alkaline oxidation; electrochemical technique; surface passivation

1. Introduction

Nowadays, about 60% ~70% of the world's gold resource reserves belong to refractory gold sources, and the total gold produced from refractory gold ores accounts for roughly 30% in the world. The micro-fine disseminated gold ore is one of the main types of refractory gold ore [1].

The pre-oxidation treatment methods of refractory gold ore containing sulfur and arsenic can be roughly divided into three categories: Roasting oxidation, biological oxidation and wet chemical oxidation. Roasting oxidation method is the most widely used in industry, but it has the major defects in the production process: Firstly, the roasting process not only has high cost, but also produces a large amount of sulfur and arsenic oxides, which are discharged into the air and cause serious pollution; Second, the following cyanide leaching process uses highly toxic cyanide, and the residue of cyanide in the discharged wastewater and tailings also has the problem of toxic pollution. The biological oxidation method has the advantages of friendly production environment, strong adaptability and stable and reliable operation of production process, but also has the disadvantages of long oxidation cycle, high requirements for process equipment and the need to adjust alkalinity in subsequent cyanide leaching, which directly leads to high production cost. Chemical oxidation can be roughly divided into alkali and acid pretreatment methods according to different pH values of pulp, and can be divided into atmospheric pretreatment and hot pressing pretreatment according to different reaction pressure conditions. Acid method and hot-pressing method have the disadvantages of high cost, high equipment requirements (acid corrosion resistance), difficult process control (high pressure danger), immature waste liquid recycling technology and environmental pollution due to the harsh conditions such as pressurization, heating and acidity, etc., so they are less

 doi:10.20944/preprints202307.0388.v1

applied in production. However, because of the advantages of low equipment requirement, low production cost, easy process control and less environmental pollution, the alkaline pre-oxidation process at room temperature and pressure has become the hot spot of research in recent years and has a good development and application prospect.

Many research data on alkaline oxidation of sulfide ores show that the oxidation sequence of common gold-bearing sulfide ores (arsenopyrite, chalcopyrite and pyrite, etc.) in alkaline oxidation system is as follows: arsenopyrite → chalcopyrite → pyrite[2–5]. Since pyrite is relatively more difficult to be oxidized than the other sulfides, it is of great significance to study the oxidation and dissolution behavior of pyrite in alkaline environment. In this paper, the oxidation and passivation of gold-bearing pyrite in alkaline electrolyte were studied by electrochemical method.

2. Materials and Methods

2.1. Preparation of massive pyrite electrode

Massive pyrite electrodes are mainly used to reasearch the corrosion and passivation process generating on surface of pyrite. The electrode requires not only high pyrite mineral purity, but also a large crystal size, no crack defect, and a smooth surface finish after grinding. Cut and grind the above-mentioned blocky pyrite into a square sheet with an area of 10x10 mm^2 and a thickness of 3～5 mm, embed it in a special square electrode casing, and seal the contact parts around with sealant to ensure that one side of the pyrite electrode contacts the electrolyte and that the pyrite is in good contact with the electrode copper wire through the electrode casing. To improve the smoothness and freshness of the electrode's surface, it is polished by using polishing powders of 10, 5, and 1 μm in sequence before electrochemical measurement, then the electrode is cleaned with ultrapure water and acetone, and finally the electrode is blown dry by argon gas and coated with a film in vacuum for standby.

2.2. Electrochemical device and supporting electrolyte

In this experiment, a cylindrical glass reactor with a capacity of 200 ml and an electrolyte of NaOH solution were used as the electrolytic cell for the electrochemical reaction test. During the test, a small amount of inert electrolyte, Na_2SO_4 was also added to increase the conductivity of the electrolyte and lower the liquid contact potential. Electrochemical measurements were performed using a three-electrode system. The working electrode was the previously prepared block pyrite electrode, the counter electrode was a platinum electrode with an area of 1 cm^2, and the reference electrode was the Hg/HgO electrode (filled with 1 M KOH). Unless otherwise stated, all potentials reported in this work are relative to Hg/HgO electrode(0.098 V vs. SHE at room temperature). The Autolab PGSTAT204 (Holland) electrochemical workstation was used for the electrochemical measurements. The measurement data is automatically collected by computer. The electrochemical test system (AUTOLAB) used in the tests is shown in Figure 1.

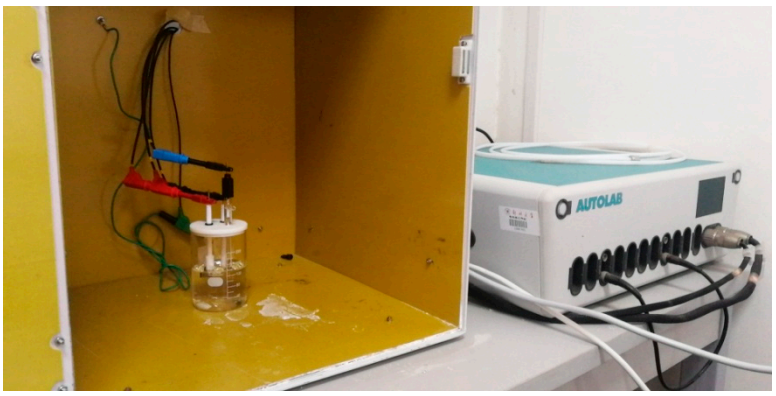

Figure 1. The AUTOLAB for the experiment.

Preprints (www.preprints.org) | NOT PEER-REVIEWED | Posted: 6 July 2023 doi:10.20944/preprints202307.0388.v1

2.3. Electrochemical tests

Four vaious electrochemical testing techniques were used in the experiments, namely cyclic voltammetry (CV), linear scanning voltammetry (LSV), current-time (i-t), and electrochemical impedance spectroscopy (EIS). Prior to each electrochemical measurement, the working electrode was maintained in the electrolyte for 30 minutes in order to ensure stability or reproducibility.

After the working electrode was immersed in electrolyte for 1 hour, the open-circuit potential (E_{OCP}) was measured by electrochemical workstation with a sampling time interval of 1 s for 30 minutes. LSV analysis was performed from E_{OCP} to an applied potential of 1.4 V at a scan rate of 0.01 V/s. CV analysis was performed between -2 V and 0.5 V at a scan rate of 0.01 V/s. Tafel polarization curve experiments were carried out in an electrolyte with a pH of 12, a voltage measurement range of -0.5 to 0.4 V, and a scan rate of 0.01 V/s. With a holding time of 10 hours, the i-t curves were measured at constant potentials of 0.4 V, 0.6 V, 0.8 V, 1.0 V, and 1.2 V, respectively. EIS curves were recorded in the frequency range of 0.05～10^5 Hz at potentials of 0.2 V, 0.4 V, 0.6 V, and 0.8 V in the electrolyte with an pH of 12. EIS data were fitted by using the software of ZSimpwin 3.60 (2014).

2.4. X-ray photoelectron spectroscopy (XPS) analysis

XPS analysis was performed by using a Thermo Escalab 250XI spectrometer under ultra-vacuum conditions (2×10^{-9} Torr) with an Al-Kα light source (hv = 1486.6 eV), operating voltage of 15 kV, a power of 25 W, and a temperature of 25 °C. The samples were analyzed using full spectrum scanning as well as fine spectrum scanning during the test, and the binding energies of the characteristic peak of all elements measured were corrected by using C1s as a reference.

3. Results

3.1. SEM analysis of original pyrite electrodes

SEM analysis of the surface of the original pyrite electrode without oxidation reaction was performed, and the result is shown in Figure 2. The surface of the pyrite electrode after grinding, polishing, and cleaning treatment is smooth, with occasional shadow spots, which may be caused by some impurities and lattice defects, and the EDS analysis result shows that the elemental content of S is 53.29% and the elemental content of Fe is 46.71%, which is basically consistent with the elemental composition of pure pyrite.

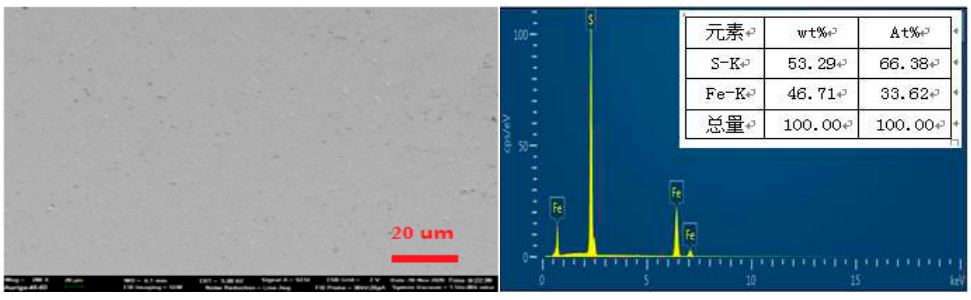

Figure 2. SEM and EDS analysis results of pyrite electrode surface.

3.2. Open circuit potential(E_{ocp}) measurement

In order to confirm the stability of the electrochemical test system, the pyrite electrode was immersed in the constantly stirred electrolyte with a temperature of 25 °C and pH value ranging from 9 to 14 for 1 hour, and then E_{ocp} test was carried out. The test results are shown in Figure 3.

Preprints (www.preprints.org) | NOT PEER-REVIEWED | Posted: 6 July 2023 doi:10.20944/preprints202307.0388.v1

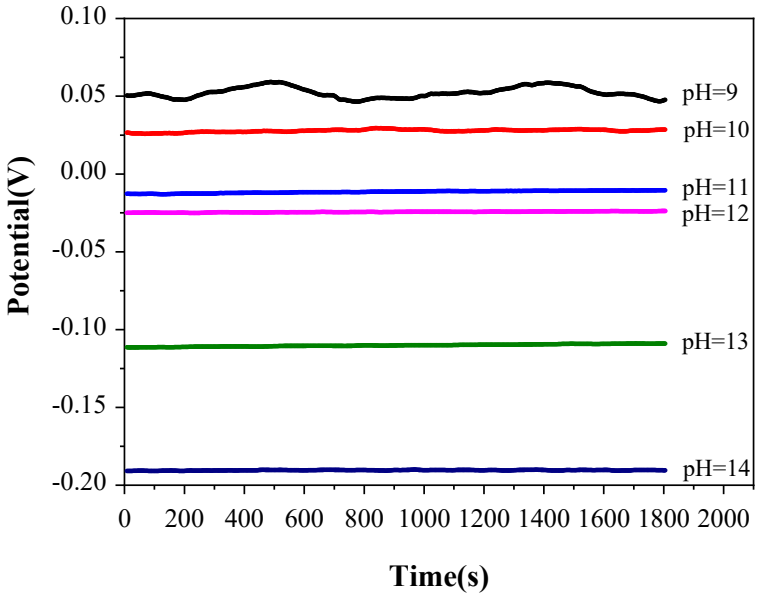

Figure 3. E_{ocp} of pyrite electrodes recorded in electrolyte of various pH value for 0.5 h.

According to Figure 3, the E_{ocp} value is relatively unstable when the pH of electrolyte is 9, which may be due to the weak potential difference fluctuation of the electrolyte caused by agitation, and the potential difference fluctuation cannot be ignored when the concentration of OH^- in the electrolyte is too low. When the pH value of electrolyte is between 10 and14, the variation of E_{ocp} with time is less than 2 mV, which indicates that the electrochemical testing system is relatively stable in this range of pH value. Therefore, the variation of the subsequent electrochemical test data is only caused by the alkaline oxidation reaction of pyrite electrode. Furthermore, E_{ocp} decreases with the increase of pHvalue in the electrolyte, which may be caused by a spontaneous oxidation reaction between pyrite and electrolyte when the electrochemical test system is in the open circuit state. with the increase of concentration of $S_x^{2-}$and $S_2O_3^{2-}$produced by pyrite oxidation in electrolyte, the oxidation potential moves to negative direction continuously.

3.3. Cyclic voltammetry (CV) measurement

CV curves were recorded in Figure 4 at a scan rate of 0.01 V/s in various pH value electrolytes, with the pH value of the electrolyte being adjusted to 10, 11, 12, and 13 with NaOH, respectively, a scan voltage of -2 V to 0.5 V, and a temperature of 25°C. The number of scan turns was five, and the fourth scan turn's results were used for data analysis.

Preprints (www.preprints.org) | NOT PEER-REVIEWED | Posted: 6 July 2023 doi:10.20944/preprints202307.0388.v1

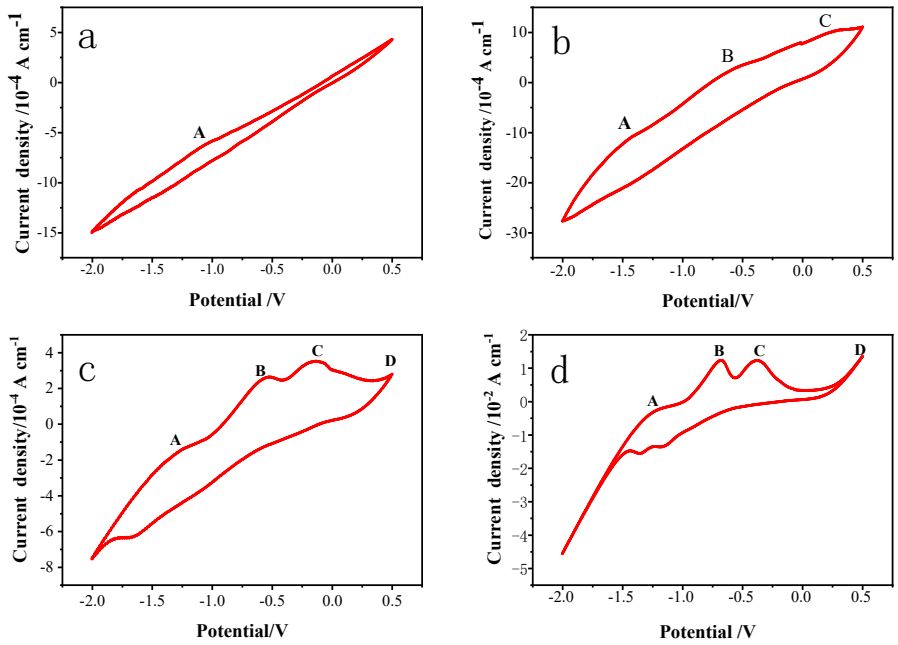

Figure 4. Typical voltammetry curve recorded of pyrite electrode in alkaline electrolyte at different pH values. (a) pH=10; (b) pH=11; (c) pH=12; (d) pH=13.

With the increase of electrolyte pH from 10 to 13, four electrochemical reaction anode peaks A, B, C, and D gradually appeared on the CV curves (Figure 4), and the reaction intensity gradually increased, which indicated that the oxidation intensity on the surface of pyrite electrode was positively correlated with the electrolyte concentration. The oxidation peaks at B, C, and D were more obvious, which indicated that the oxidation intensity on the surface of -pyrite electrode was also positively correlated with voltage. Furthermore, the oxidation peak potential gradually moved to the negative potential with the increase of electrolyte pH, which indicated that the higher the pH value, the easier the oxidation reaction.

Because the reaction voltage is low and the oxidation intensity is weak, the chemical reaction (1) appears to take place primarily at the anode peak A, according to the available data [6,7]. At this point, the Fe-S bond in FeS_2 is broken to form $Fe(OH)_2$ and S_M, with $Fe_{1-x}S_2$ and S_x^{2-} being the main components of S_M. The pyrite electrode continues to be oxidized as the oxidation voltage increases, and the anodic peak at B can be explained by the reaction equation (2), which states that $Fe(OH)_2$ is further oxidized to $Fe(OH)_3$, and the main components of S_L are S^0 and minor amounts of $Fe_{1-x}S_2$ and S_x^{2-}. While, the anodic peak at C can be explained by the reaction equation (3), which states that $Fe(OH)_2$ is further oxidized to $Fe(OH)_3$, and the main components of S_L are further converted to SO_3^{2-}. Interestingly, when the CV curves at pH 13 and 14 are scanned at 0.50 V, a clear sharp oxidation peak D appears, owing to pyrite's high oxidation reaction rate at relatively high voltages. Two chemical reactions occured on pyrite electrode at this high voltage: one is the oxidation reaction of pyrite itself to form $Fe(OH)_3$ and SO_4^{2-} (Eq.4), and the other is the process of re-oxidation of the surface oxidation product SO_3^{2-} formed at low voltage to form SO_4^{2-} (Eq.4).

$FeS_2 + 2H_2O \rightarrow Fe(OH)_2 + 2S_M + 2H^+ + 2e^-$ (1)

$FeS_2 + 3H_2O \rightarrow Fe(OH)_3 + 2S_L + 3H^+ + 3e^-$ (2)

$S_L + 3H_2O \rightarrow SO_3^{2-} + 6H^+ + 6e^-$ (3)

$FeS_2 + 11H_2O \rightarrow Fe(OH)_3 + 2SO_4^{2-} + 19H^+ + 15e^-$ (4)

$SO_3^{2-} + H_2O \rightarrow SO_4^{2-} + 2H^+ + 2e^-$ (5)

The reduction peak of pyrite bulk electrode is not apparent when scanned from 0.50 V to low potential, and the weak reduction peak can be observed only at pH 12 . It is inferred that the oxidation product $Fe(OH)_3$ is reduced to Fe^{2+} occurs between -1.4 V and -1.6 V when pH is 13 or 14. (as shown in Eq.6). There is a smaller reduction peak subsequently, which may indicate that pyrite or its

Preprints (www.preprints.org) | NOT PEER-REVIEWED | Posted: 6 July 2023 doi:10.20944/preprints202307.0388.v1

products are directly reduced to form H_2S or ferrous sulfides (Eq.7). The analysis of the electrolyte composition also reveals a low concentration of S^{2-} existed in the electrolyte solution.

$Fe(OH)_3 + 3H^+ + e^- \rightarrow Fe^{2+} + 3H_2O$ (6)

$FeS_2 + 2H^+ + 2e^- \rightarrow FeS + H_2S$ (7)

3.4. Linear sweep voltammetric curve (LSV) measurements

The LSV curve test of the pyrite electrode was conducted in an electrolyte of pH12 and 25°C. The test voltage was from 0 V to 1.4 V and the scan rate was 0.01 V/s. The test result is shown in Figure 5.

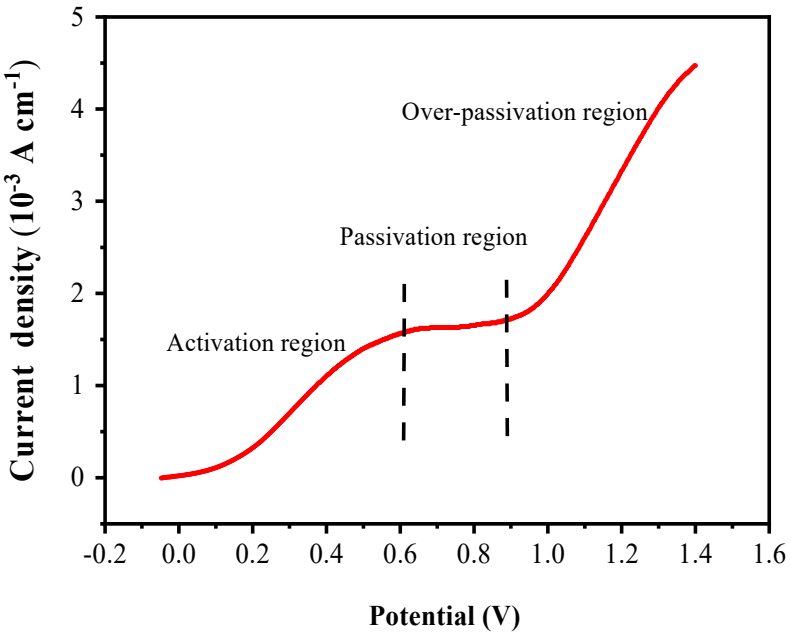

Figure 5. LSV curve recorded of pyrite electrode in alkaline solution of pH12.

In this LSV curve, three distinct rigions can be divided: active region, passive region, and over-passive region, as shown in Figure 5. In the active region between 0 and 0.6 V, the current density increases rapidly with the increase of voltage, which is likely due to the oxidative dissolution of pyrite in this voltage range. In the passivation region between 0.6 and 0.9 V, the current density is almost constant, and the response to the voltage increase is not obvious, this may be because oxidation products of pyrite, such as $Fe(OH)_2$, $Fe(OH)_3$ and so on, deposit on the electrode surface to form a passivation layer, which prevents the current density from continuing to increase with the voltage increase. In the over-passivation region of 0.9~1.4 V, the current density increases rapidly again with the increase of voltage. This is likely because when the voltage increases to 0.9 V, the high voltage provides a stronger driving force for the reaction to break down the passivation layer, so the pyrite covered by the passivation layer can continue be oxidized.

3.5. i-t curve measurements

The results of CV and LSV demonstrate that the oxidative dissolution of pyrite occurs over a broad range of voltages. To determine the accumulation of products on the surface of pyrite over time and to observe the oxidative dissolution on the surface of pyrite, an i-t curve test was performed at pH 12 and 25 °C for the pyrite electrode at test voltages of 0.4 V, 0.6 V, 0.8 V, and 1.0 V, respectively. The results were showed in Figure 6.

Preprints (www.preprints.org) | NOT PEER-REVIEWED | Posted: 6 July 2023 doi:10.20944/preprints202307.0388.v1

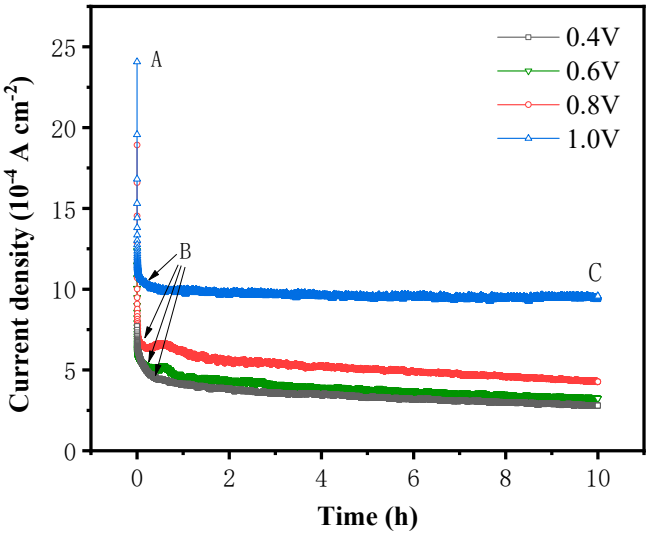

Figure 6. The i-t curves of pyrite electrode after alkaline oxidation at different voltages

As depicted in Figure 6, at all four potentials, the current densities finally tended to be steady at the lower value after dropping acutely within first several decades minutes. The variation of current density with reaction time can be roughly divided into two stages, AB and BC. In AB stage, initial current density increases with the rising of applied potential, while the current density decreases rapidly as the reaction time. In BC stage, the current density tended to be stable with the increase of reaction time. In addition, the higher the system potential and relatively the stable current density is also higher.

As the electrochemical oxidation reaction occurs on the surface of the pyrite electrode under the action of the applied potential, the reaction products rapidly accumulate on the surface of the pyrite and form a passivation layer, which hinders the reaction to a certain extent, resulting in a rapid decrease of current density in AB stage. In addition, the increase in voltage accelerates the decrease in current density in AB stage because the higher the voltage, the faster the oxidation and dissolution rate of pyrite, the faster the formation of the passivation layer on the surface of pyrite per unit time, and the greater the degree of hindrance to the reaction.

When the potential was between 0.4 V and 0.8 V, the current density in BC stage increased slightly with an increase in voltage and decreased with time. This may be because the passivation layer formed in AB stage failed to completely prevent the oxidation reaction from proceeding, resulting in the accumulation of the passivation layer with the extension of the reaction time and the gradual deepening of the impeded reaction, so the current density showed a gradual decrease with time. When the potential reaches 1.0 V, the current density in BC stage basically does not change with time, indicating that the oxidation reaction is faster in AB stage under high potential conditions, and the passivation layer can quickly reach the thickness that prevents the reaction from proceeding, which in turn makes the reaction rate in BC stage extremely slow, and the hindering effect of the passivation layer on the reaction also remains stable, and the current density also tends to be stable.

3.6. Electrochemical impedance spectroscopy analysis

EIS test was conducted at a pH level of 12 and a temperature of 25°C. The frequency scanning range was 0.01~1 × 10^5 Hz, and the amplitude was 5 mV. The fitted Nyquist plots by equivalent circuits at specific potentials of 0.5, 0.6, 0.7 and 0.8 V in alkaline electrolyte are shown in Figure 7. Fitting parameters of the equivalent circuits simulated from the EIS are shown in Table 1.

Preprints (www.preprints.org) | NOT PEER-REVIEWED | Posted: 6 July 2023 doi:10.20944/preprints202307.0388.v1

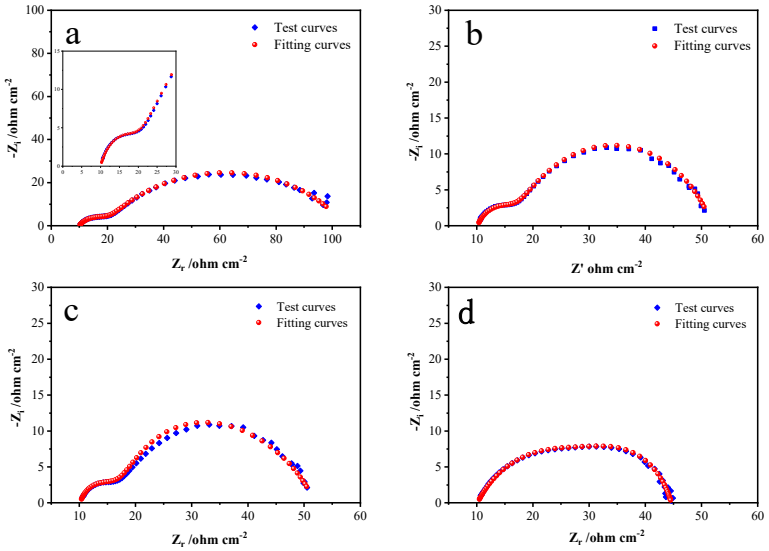

Figure 7. The measured and calculated Nyquist plots of pyrite electrodes at different anodic potentials in an alkaline supporting electrolyte (a: 0.2 V, b: 0.4 V, c:0.6 V, d: 0.8 V).

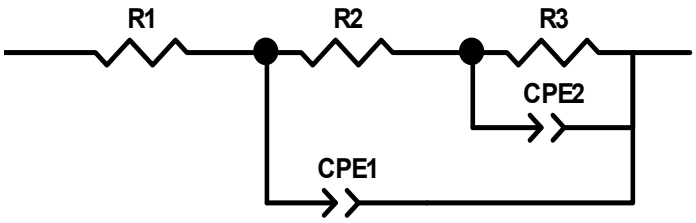

Figure 8. Equivalent circuit models used for fitting measured EIS data（R1, solution resistance; R2, polarization resistance generated by the interface capacitor CPE1; R3, charge transfer resistance）

As can be seen from Figure 7, a small semicircular arc and a large one appear successively in the high frequency region and the middle frequency region. The small semicircular arc in the high frequency region corresponded to capacitance related to electrode-solution interface, and the large semicircle arc in the middle frequency region is generated by the Heimholtz double capacitance layers on the pyrite electrode surface According to Figure 5 and Figure 6, When the system potential is between 0.2 and 0.6 V, the pyrite electrode is in an activation zone during the alkaline oxidative dissolution process, the reaction products have not yet formed a stable passivation layer on the electrode surface, and the electrochemical reaction is active, which means that the passivation layer is not enough to hinder the chemical oxidation reaction and the electrode reaction rate is primarily controlled by the electrochemical reaction. The deviation of the small semicircular arc in Figure 7 from the standard semicircular state is due to the polarization of the electrode surface as the frequency decreases, and the chemical reation caused by the polarization also results in another larger arc until the S^0 and $Fe(OH)_3$ generated during the chemical reaction adsorbs on the electrode surface to form a passivation layer, and as the passivation layer thickens, it finally leads to the chemical reaction to stop and the real and imaginary parts are basically no longer changeable. For the same reason there is no Warburg impedance characteristic slope line with the representation of the diffusion process in the impedance diagram's low and middle frequency regions. As the potential continues to rise to 0.8 V, the distinction between the small and large semicircular arcs becomes no longer obvious, this is because the chemical reaction process accelerates at higher potentials, obscuring the surface polarization of the electrode.

Figure 8 presents the equivalent circuit models used to fit the measured EIS data, where R1 represents the solution resistance, R2 represents the interface polarization resistance, capacitance CPE1, R3 represents the charge transfer resistance. Based on the test and fitted curves in Figure 7, the fitted data match with the experimental data closely when this circuit is used, which indicates the

Preprints (www.preprints.org) | NOT PEER-REVIEWED | Posted: 6 July 2023 doi:10.20944/preprints202307.0388.v1

equivalent circuit model can better reflect the dynamical behaviors of the bulk pyrite electrode more accurately during the alkaline oxidation process.

Table 1. Fitting parameters of the equivalent circuits simulated from the EIS in Figure 7

U（V）	0.2（V）	0.4（V）	0.6（V）	0.8（V）
R_1(Ω cm^{-2})	10.02	10.12	10.32	10.16
R_2(Ω cm^{-2})	12.07	8.49	21.35	25.56
R_3(Ω cm^{-2})	82.04	34.34	17.48	9.163
CPE_1-T(F cm^{-2})	0.0021609	0.0014452	0.001271	0.0089737
CPE_1-P(F cm^{-2})	0.67268	0.72403	0.78395	0.89019
CPE_2-T(F cm^{-2})	0.00016282	0.00016892	0.00023613	0.00031208
CPE_2-P(F cm^{-2})	0.69829	0.69665	0.66611	0.64281

Table 1 lists the parameter values of the equivalent circuit model (Figure 8) at different potentials. The charge transfer resistance R_3 decreases from 82.04 cm^{-2} to 9.163 cm^{-2} as the system's reaction voltage rises from 0.2 V to 0.8 V. As the reaction voltage increases, R3 decreases, the charge transfer rate during the reaction increases, and the alkaline oxidative dissolution reaction of pyrite occurs more rapidly. As shown in Figure 7, the rate rises while the radius of the semicircular arc falls. The constant phase element dispersion index (CPE_2-T), which reflects how far the corresponding capacitance deviates from the ideal capacitance, is typically used. According to Table 1, the CPE_2-T gradually rises as the voltage rises. This may be because as the voltage rises, the electrode surface's reaction rate rises and more S^0 and $Fe(OH)_3$ accumulate on the electrode surface, which causes the electrode surface's roughness to rise and, in turn, raises the CPE_2-T.

3.7. XPS analysis

XPS technique was applied to identify the iron and sulfur oxidation products on the bulk pyrite electrode surface after 10 h of the i-t curve test at potentials of 0.4 V, 0.6 V, 0.8 V, and 1.0 V. The measured and fitted plots are shown in Figure 9 and the fitting parameters are present at Table 2.

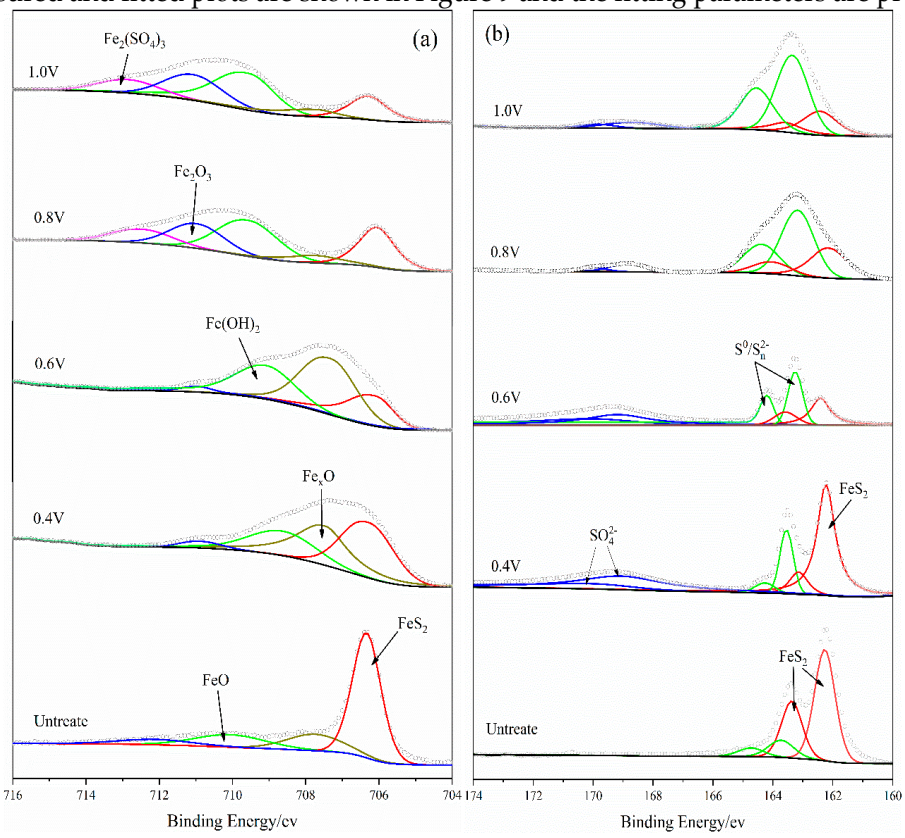

Preprints (www.preprints.org) | NOT PEER-REVIEWED | Posted: 6 July 2023 doi:10.20944/preprints202307.0388.v1

Figure 9. Iron and sulfur XPS spectrums of pyrite electrodes for unreacted and chronoamperometry treated (a: $Fe_{2P3/2}$ spectrum of pyrite electrodes; b: S_{2P} doublets spectrum of pyrite electrodes).

Table 2. Fitting parameters of XPS spectrums in Figure 9

Spectrum	Original mineral	0.4V	0.6V	0.8V	1.0V	Interpretation
$Fe_{2p3/2}$	706.30	706.34	706.38	706.40	706.50	FeS_2
	707.82	707.88	707.90	707.91	707.93	Fe_xO
	710.0	709.10	709.51	709.80	709.82	$FeO/ Fe(OH)_2$
		710.8	710.84	710.85	710.90	$Fe_2O_3/FeOOH$
				713.12	713.25	$Fe_2(SO_4)_3$
$S_{2p3/2}$	162.20	162.23	162.35	162.24	162.35	FeS_2
	163.80	163.72	163.42	163.70	164.05	S^0/S_n^{2-}
		168.48	168.25	168.40	168.52	SO_4^{2-}

The $Fe_{2p3/2}$ spectra of unreacted and anodic-reacted pyrite electrodes are shown in Figure 9(a), five characteristic peaks appeared at 706.3 eV, 707.82 eV, 710.0 eV, 710.8 eV and 713.12 eV for different reaction voltages. The peak with a binding energy of 706.3 eV was considered to correspond to FeS2 [8–10]. The peak at 707.82 eV was corresponded to be Fe_xO with an iron valence betwen 0 and +2, which gradually transforms to divalent or trivalent iron as the oxidation potential increases. The peaks at 710.0 eV and 710.8 eV were corresponded to $FeO/Fe(OH)_2$ and $Fe_2O_3/FeOOH$, respectively [11–13]. It was possible that both iron oxides and hydroxides existed on the surface of the pyrite electrode because of the alkaline oxidation environment and the ultravacuum environment during XPS detection. Iron hydroxides may be partially dehydrated to become iron oxides under the super vacuum conditions. Another peak at 713.12 eV was corresponded to $Fe_2(SO_4)_3$ [14], which was difficult to be detected at low oxidation potentials because of its solubility. When the oxidation potential increased, a large amount of $Fe_2(SO_4)_3$ products didn't diffuse into the solution in time and produced a small amount of deposition on the electrode surface, which was then detected. In conclusion, these stronger peaks at strong oxidation potentials indicated that the presence of a large amount of Fe(III) in forms of $Fe(OH)_3$, FeOOH, Fe_2O_3 or $Fe_2(SO_4)_3$on the surface of the pyrite electrode due to electrochemical polarization, which was consistent with the conclusions of the discussed electrochemical measurements.

Figure 9(b) shows S_{2p} spectra of the pyrite electrode before and after the oxidation reaction. The dominant peak at the binding energy of 162.2 eV was corresponded to FeS_2 [8,9,15] . The intensity of the oxidation reaction increased with increasing voltage, and the thickness of the passivation layer, which was resulted from the accumulation of adhesion products on the surface of the pyrite electrode, increased rapidly, therefore, the intensity of the FeS_2 characteristic peak decreased gradually. The peak at 163.8 eV was supposed to be S_0 or S_x^{2-} [10,16–18] , and the faint peak at 168.42 eV was considered to be SO_4^{2-} [9,14,19], which may be the final oxidation products of S in pyrite.

3.8. SEM and EDS analysis

In order to observe the passivation layer formed on the surface of pyrite electrode, the bulk pyrite electrode were subjected to chronoamperometry measurements at 0.8 V with various reaction times of 10 min, 20 min, 30 min, 40 min, 50 min, 60 min, 120 min, 180 min, and 240 min in an alkaline electrolyte of pH12 and 25 °C. The tested pyrite electrodes were subsequently analyzed by SEM and EDS, and the results are showed in Figure 9 and Figure 10.

Preprints (www.preprints.org) | NOT PEER-REVIEWED | Posted: 6 July 2023 doi:10.20944/preprints202307.0388.v1

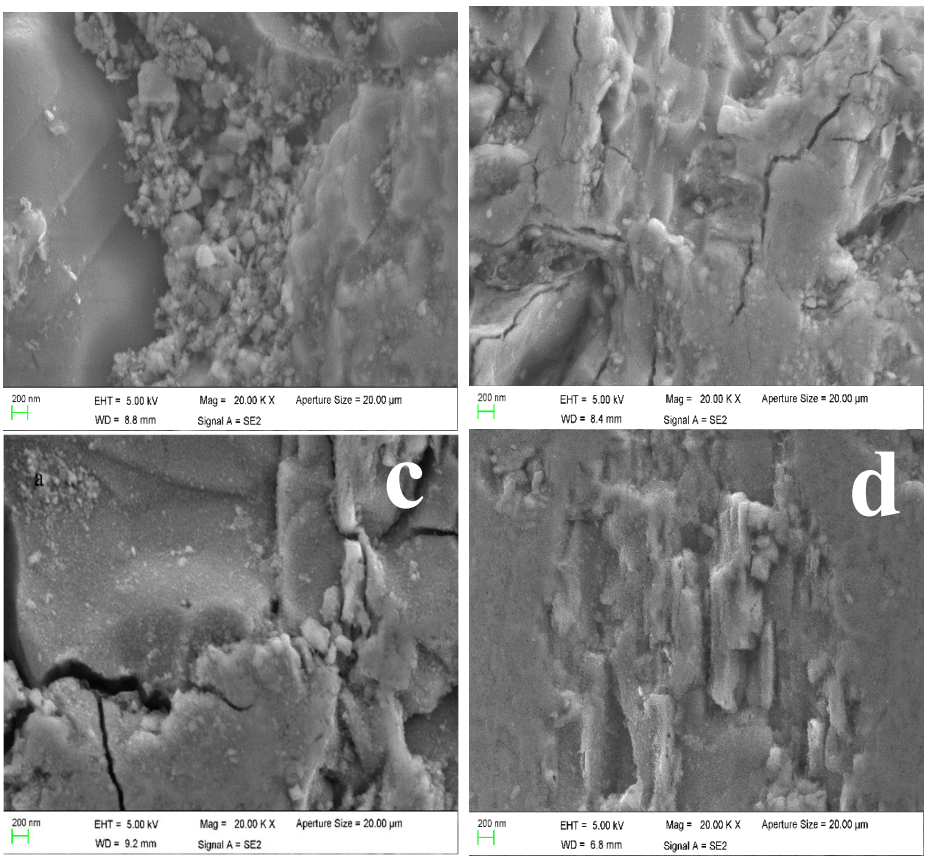

Figure 10. SEM images of pyrite electrode surface at different reaction times((a) 10 min; (b) 60 min; (c) 120 min; (d) 240 min).

When the reaction time was 10 min, the oxidation-dissolution reaction occurred primarily on the surface, and a small amount of oxidation product accumulation could be seen on the electrode surface, which was not completely covered. It was evident from Figure 10(a) that there were only a few slight corrosion pits on the surface of the pyrite electrode and no obvious passivation layer was formed. For the reaction time of 60 min, the passivation layer formed by the oxidation products completely covered the electrode surface and contained microcracks (Figure 10(b)). For the reaction time of 120 minutes, the reaction products continued to accumulate on the surface, the passivation layer appeared as blocky aggregates, the blocky crack traces deepened, and the blocky area grew, indicating that the passivation degree increased (Figure 10(c)). When the pyrite electrode continued to react for 240 min, the surface cracks of the passivation layer were filled with new reaction products, the oxidation reaction of pyrite electrode basically stopped and the accumulation of the passivation layer slowed or ceased (Figure 10(d)).

Preprints (www.preprints.org) | NOT PEER-REVIEWED | Posted: 6 July 2023 doi:10.20944/preprints202307.0388.v1

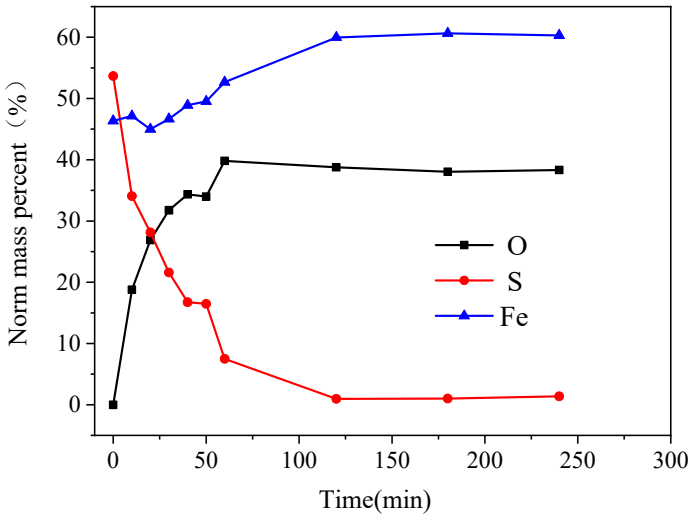

Figure 11. Variation of O, S, Fe content of pyrite electrode surface with time.

The content of O and Fe elements in the oxidation products on the surface of the pyrite electrode increases as the reaction time increases, while the content of S elements decreases. In 0-60 min, the elemental content of S decreased rapidly from 53.66 % to 7.55 %, the elemental content of O increased rapidly from 0% to 39.81%, and the elemental content of Fe first decreased slightly and then increased gradually. The changes of O, S, and Fe elemental contents on the surface of the pyrite electrode slowed after 60 min and stabilized after 120 min. During electrochemical oxidation and decomposition of pyrite, S element mainly entered the electrolyte in the form of ions, which didn't deposit on the electrode surface easily, so the S element content decreases rapidly. , A small portion of Fe elements entered the solution in the form of soluble $Fe(OH)^{+}$ after being oxidized, so the Fe content decreases initially. However, because the electrolyte was strongly alkaline, $Fe(OH)^{+}$ continued to react with OH^{-} as its concentration increased, the passivation layer gradually was formed on the electrode surface as $Fe(OH)_3$, and as the passivation layer gradually thickens over time, its composition tended to remain stable.

3.9. Ion content change pattern in electrolyte

The oxidation reaction of the pyrite electrode was carried out in an alkaline electrolyte at pH 12 and 25 °C at different voltages and times, and the reacted electrolyte was analyzed for ionic composition; the results are shown in Figure 12.

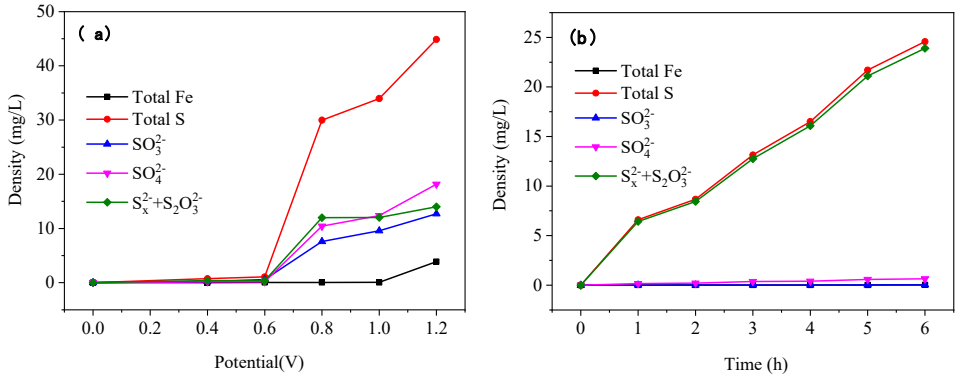

Figure 12. Changes of ion content in electrolytes under different reaction conditions. (a) The ionic compositions of the electrolytes in which the pyrite electrode reacted for 10 hours at different potentials. (b) The ionic compositions of the electrolytes in which the pyrite electrode reacted at 0.8 V potential for different oxidation times.

 doi:10.20944/preprints202307.0388.v1

As the reaction voltage increased, the S content in the electrolytes increased significantly, while the Fe content increased only slightly (Figure 12(a)). This is because S element enters the electrolyte in the ionic state when the pyrite is oxidized and dissolved, whereas Fe element finds it is difficult for Fe to exist in the strong alkaline electrolyte in form of the ions. The contents of SO_3^{2-}, SO_4^{2-}, and (S_x^{2-} + $S_2O_3^{2-}$) ions increased significantly as the reaction voltage rose, with the increase of (S_x^{2-} + $S_2O_3^{2-}$) being greater than that of SO_3^{2-} and SO_4^{2-}. During the oxidative dissolution of pyrite, S element was oxidized and converted to S_x^{2-} and $S_2O_3^{2-}$ before being further oxidized to SO_3^{2-} and SO_4^{2-}, resulting in a greater increase of S_x^{2-} and $S_2O_3^{2-}$ than of SO_3^{2-} and SO_4^{2-}. Moreover, since S_x^{2-} and $S_2O_3^{2-}$ are in the unstable intermediate states, increasing the reaction voltage can accelerate the conversion of (S_x^{2-} + $S_2O_3^{2-}$) to SO_3^{2-} and SO_4^{2-}, as evidenced by the increase in SO_3^{2-} and SO_4^{2-} concentration with increasing voltage.

The content of S in the electrolyte increased significantly as reaction time increased, while the content of Fe element remained essentially unchanged (Figure 12(b)). This is due to the fact that The Fe ions produced by oxidation in the strong alkaline electrolyte quickly formed iron hydroxide which was deposited on the surface of pyrite electrode, therefore, the ionic iron content in the electrolyte is very low. With an increase in reaction time, the content of SO_3^{2-} and SO_4^{2-} was low and did not change significantly, whereas the content of (S_x^{2-} +$S_2O_3^{2-}$) was high, indicating that under suitable alkaline oxidation conditions, S_x^{2-} and $S_2O_3^{2-}$ produced by the pyrite oxidation reaction can exist steadily in the solution, which is the basis for gold leaching by using pyrite's own oxidation products.

4. Conclusions

In this paper, the oxidation process of the pyrite in alkaline electrolyte was studied by the electrochemical testing technique, and the oxidation products of pyrite electrode in alkaline electrolyte were characterized by combining various analytical testing methods, such as XPS and SEM. The conclusions of the study are as follows.

(1) The electrochemical oxidative dissolution of pyrite occurs best in an alkaline environment with a pH of around 12, and an appropriate oxidation potential is one above 0.8 V. These parameters are still of reference significance in the pre-oxidation treatment process of sulfide ores by chemical oxidants.

(2) During the alkaline oxidative dissolution of pyrite, some element S enters the electrolyte as S_x^{2-}, $S_2O_3^{2-}$, SO_3^{2-}, and SO_4^{2-} ions, and a small amount of element S is adsorbed on the electrode surface as S^0 to form the passivation layer. As the main component of the passivation layer, Fe is essentially adsorbed on the electrode surface as $Fe(OH)_2$, Fe_2O_3, and $Fe_2(SO_4)_3$.

(3) When the oxidation potential is between 0 and 0.6 V, the increase in reaction voltage has no discernible effect on the change in ion concentration in the electrolyte. Low potential polarization could result in the formation of a sulfur-rich passivation film on the surface of pyrire electrode, which caused the reaction to slow down or stop. When the voltage is greater than 0.6 V, with the increase in potential, the inert oxidation products dissolved, the oxidation process continued, and the concentrations of soluble ions in the electrolyte began to rise rapidly. With the prolongation of reaction time, S element was first converted into S_x^{2-} and $S_2O_3^{2-}$, and then further oxidized to SO_3^{2-} and SO_4^{2-}, whereas S_x^{2-} and $S_2O_3^{2-}$ can remain stable in solution for a longer time. Therefore, the content of S_x^{2-} and $S_2O_3^{2-}$ in the electrolyte increased rapidly with the prolongation of reaction time, whereas the content of SO_3^{2-} and SO_4^{2-} changed little.

Author Contributions: Yehao Huang: Data curation, Methodology, Formal analysis, Writing – original draft. Zipei Jia: Methodology and Writing – review & editing. Wen Wang: Writing – review & editing. Jia Yao: Writing – review & editing. Runbo Gao: Writing – review & editing. Yongsheng Zhang: Supervision. Xiangyu Song: Conceptualization, Resources, Writing – review & editing, Funding acquisition.

Funding: This work was supported by the National Natural Science Foundation of China [grant number 51874259 and 52074244].

Data Availability Statement: Not applicable.

 doi:10.20944/preprints202307.0388.v1

Conflicts of Interest: The authors declare no conflict of interest.

References

1. LEI Z, XUEYI G, QINGHUA T, et al. Research progress and industrial application of pretreatment methods for refractory gold ores [J]. Gold, 2021, 42(06): 60-8.
2. CIMINELLI V. Oxidation of pyrite in alkaline solutions and heterogeneous equilibria of sulfur-and arsenic-containing minerals in cyanide solutions [J]. Colloids and Surfaces A：Physicochemical and Engineering Aspects, 1987.
3. CIMINELLI V, OSSEO-ASARE K. Kinetics of Pyrite Oxidation in Sodium Carbonate Solutions [J]. Metallurgical and Materials Transactions, 1995, 26B(2): p.209-18.
4. KHOSO S A, HU Y-H, LU F, et al. Xanthate interaction and flotation separation of H2O2-treated chalcopyrite and pyrite [J]. Transactions of Nonferrous Metals Society of China, 2019, 29(12): 2604-14.
5. TAO D P, LI Y Q, RICHARDSON P E, et al. The incipient oxidation of pyrite [J]. Colloids and Surfaces A Physicochemical and Engineering Aspects, 1994, 93(none): 229-39.
6. WENRUI J, ZHIHONG T, SHU Z, et al. A Brief Overview on the Mechanism and Kinetic Influencing Factors of the Pyrite Surface Oxidation [J]. METAL MINE, 2021, (03): 88-102.
7. XU G, DENG F, FAN W, et al. Pre-oxidation of refractory gold concentrate by electrochemical methods in alkaline electrolyte [J]. Materials Today Communications, 2022, 31.
8. NAVEAU A, MONTEIL-RIVERA F, GUILLON E, et al. XPS and XAS studies of copper(II) sorbed onto a synthetic pyrite surface [J]. Journal of Colloid and Interface Science, 2006, 303(1): 25-31.
9. NESBITT H W, BANCROFT G M, PRATT A R, et al. Sulfur and iron surface states on fractured pyrite surfaces [J]. American Mineralogist, 1998, 83(9-10): 1067-76.
10. WITTSTOCK G, KARTIO I, HIRSCH D, et al. Oxidation of galena in acetate buffer investigated by atomic force microscopy and photoelectron spectroscopy [J]. Langmuir, 1996, 12(23): 5709-21.
11. EJTEMAEI M, NGUYEN A V. Characterisation of sphalerite and pyrite surfaces activated by copper sulphate [J]. Minerals Engineering, 2017, 100: 223-32.
12. YANG X, MU Y, PENG Y. Comparing lead and copper activation on pyrite with different degrees of surface oxidation [J]. Minerals Engineering, 2021, 168.
13. ZHANG T, WANG Y, HU Y, et al. HO center dot selective cleavage Fe-S bond for FeS2 electrolysis in alkaline solution [J]. Electrochimica Acta, 2019, 306: 327-38.
14. TU Z, WAN J, GUO C, et al. Electrochemical oxidation of pyrite in pH 2 electrolyte [J]. Electrochimica Acta, 2017, 239: 25-35.
15. DERYCKE V, KONGOLO M, BENZAAZOUA M, et al. Surface chemical characterization of different pyrite size fractions for flotation purposes [J]. International Journal of Mineral Processing, 2013, 118: 1-14.
16. BUCKLEY A N, WOODS R. THE SURFACE OXIDATION OF PYRITE [J]. Applied Surface Science, 1987, 27(4): 437-52.
17. HAMPTON M A, PLACKOWSKI C, NGUYEN A V. Physical and Chemical Analysis of Elemental Sulfur Formation during Galena Surface Oxidation [J]. Langmuir, 2011, 27(7): 4190-201.
18. NIU X, CHEN J, LI Y, et al. Correlation of surface oxidation with xanthate adsorption and pyrite flotation [J]. Applied Surface Science, 2019, 495.
19. CAI Y F, PAAN Y G, XUE J Y, et al. Comparative XPS study between experimentally and naturally weathered pyrites [J]. Geochimica Et Cosmochimica Acta, 2009, 73(13): A184-A.